

# Colour centres and nanostructures on the surface of laser crystals

N.A. Kulagin

**Abstract.** This paper presents a study of structural and radiation-induced colour centres in the bulk and ordered nanostructures on the surface of doped laser crystals: sapphire, yttrium aluminium garnet and strontium titanate. The influence of thermal annealing, ionising radiation and plasma exposure on the spectroscopic properties of high-purity materials and crystals containing Ti, V and Cr impurities is examined. Colour centres resulting from changes in the electronic state of impurities and plasma-induced surface modification of the crystals are studied by optical, EPR and X-ray spectroscopies, scanning electron microscopy and atomic force microscopy. X-ray line valence shift measurements are used to assess changes in the electronic state of some impurity and host ions in the bulk and on the surface of oxide crystals. Conditions are examined for the formation of one- and two-level arrays of ordered crystallites  $10^{-10}$  to  $10^{-7}$  m in size on the surface of crystals doped with iron-group and lanthanoid ions. The spectroscopic properties of the crystals are analysed using *ab initio* self-consistent field calculations for  $Me^{n+} : [O^{2-}]_k$  clusters.

**Keywords:** oxides, impurity ions, spectra, clusters, nanostructures.

## 1. Introduction

The structural, spectroscopic and dielectric properties of oxide single crystals, such as sapphire ( $\alpha$ - $Al_2O_3$ ), garnets ( $A_3B_2C_3O_{12}$ ) and perovskites ( $ABO_3$ ), have been the subject of extensive studies. A small part of their results can be found in Refs [1–7]. The wide diversity of properties of oxide compounds, which depend on synthesis conditions and impurity concentrations and can be changed by thermal annealing and irradiation, is associated with changes in the fundamental properties of crystals and considerable oxygen vacancy concentrations [3–13].

Doping with chromium oxide converts sapphire (an example of a binary single-crystal oxide) to ruby,  $\alpha$ - $Al_2O_3$ :Cr, the first crystalline laser material and the subject of detailed studies [1, 3, 14]. Ti-doped sapphire,  $\alpha$ - $Al_2O_3$ :Ti, has also been thoroughly studied. There is a great deal of attention focused on garnet-structure crystals owing to the wide use of such crystals in laser engineering. Perovskites are of interest because they are used in laser beam steering systems and because some properties of perovskite materials can be varied in a controlled manner, with the potential of extending their application field [14–20].

The incorporation of iron-group or lanthanoid ions, which have a partially filled 3d or 4f shell, changes the spectroscopic, electrical, dielectric and other properties of oxides and can be used to produce new materials, e.g. for lasers and photonics [1, 3–6, 16–19]. Exposure to a plasma or ionising radiation and thermal annealing in an oxidising, reducing or neutral atmosphere also change the electronic structure and properties of both undoped and doped oxide crystals [1, 18–22]. Such processing produces significant changes in the electronic spectrum, crystal structure and other properties of sapphire ( $\alpha$ - $Al_2O_3$ ), yttrium aluminium garnet (YAG,  $Y_3Al_5O_{12}$ ), gadolinium scandium gallium garnet (GSGG,  $Gd_3Sc_2Ga_3O_{12}$ ), gadolinium scandium aluminium garnet (GSAG,  $Gd_3Sc_2Al_3O_{12}$ ) and other multicomponent garnet crystals and also in those of yttrium orthoaluminate ( $YAlO_3$ ) and strontium titanate ( $YAlO_3$ ) crystals [19–26].

The large amount of information obtained in studies of materials having different impurity compositions and synthesised under different conditions makes it difficult to understand fundamental aspects of the formation of defects and colour centres in crystals.

As shown earlier [5, 27–29], exposure to ionising radiation leads under certain conditions to changes in the electronic state (valence) of iron group ions in sapphire, garnets and perovskites. There is ample evidence [5, 21, 30] for the formation of appreciable  $Ti^{3+}$  concentrations on cation sites in many  $Sr^{2+}Ti^{4+}O_3^{2-}$  samples. Changes in the electronic state of some of the host ions in strontium titanate crystals may be caused by deviations from stoichiometry or the formation of considerable oxygen vacancy concentrations during synthesis and heat treatment. In particular, the lattice parameter  $a$  of strontium titanate may vary from 3.9051 Å in stoichiometric crystals to 3.8954 Å at  $Ti^{3+}$  concentrations near 20% [31].

The action of ionising radiation and plasma flows on the surface of some oxide single crystals (both undoped and doped with iron-group or lanthanoid ions) led to the formation of colour centres and changes in the spectroscopic properties of the materials. The first experiments concerned with the influence of a high-energy plasma demonstrated the possibility of producing complex, quasi-ordered arrays of pyramid-like crystallites  $10^{-6}$  to  $10^{-10}$  m in size on oxide surfaces [31–33].

The purpose of this work was to examine general aspects of the formation of colour centres in the bulk and on the surface of crystals under the action of ionising radiation and high-temperature annealing and analyse plasma-induced changes in the surface morphology and spectroscopic properties of undoped and doped oxide single crystals. Sapphire, garnet and strontium titanate single crystals were studied mainly using experimental spectroscopic techniques and *ab initio* self-consistent field calculations for clusters and doped crystals.

N.A. Kulagin Firma SIFA Ukraine–Germany Joint Venture,  
ul. Shekspira 6-48, 61045 Kharkiv, Ukraine;  
e-mail: nkulagin@bestnet.kharkov.ua

Received 25 May 2012; revision received 11 July 2012  
Kvantovaya Elektronika 42 (11) 1008–1020 (2012)  
Translated by O.M. Tsarev

This paper presents the results of investigation concerned with the effects of thermal annealing, ionising radiation and plasma on the spectroscopic properties of undoped and iron-group metal or lanthanoid doped sapphire, ruby, yttrium aluminium garnet, gadolinium scandium gallium garnet, gadolinium scandium aluminium garnet, strontium titanate and yttrium orthoaluminate crystals prepared under various conditions. Samples for this study were prepared under various conditions and were doped with iron-group or lanthanoid ions, e.g. with Ti, V, Cr, Sm or Nd ions. We studied the influence of gamma irradiation to doses in the range  $10^2$  to  $10^4$  Gy and the formation of ordered structures  $10^{-7}$  to  $10^{-10}$  m in size under the action of a high-energy plasma.

## 2. Samples and experimental procedures

As shown in many studies, the spectroscopic properties of oxides depend on the synthesis procedure, including subsequent heat treatment, and on the concentration of unintentional impurities [4–6, 34, 35]. Given this, in the first step we examined radiation-induced changes in the spectroscopic properties of samples prepared by various techniques.

### 2.1. Samples

As in previous studies [27–29, 34, 35], sapphire, garnet and strontium titanate crystals were grown by the Verneuil process, Czochralski pulling, horizontal and vertical directional solidification and other methods. The growth of sapphire and strontium titanate crystals by the Czochralski and Verneuil processes is well known and has been described in detail elsewhere [5, 21, 22, 34]. Garnet and yttrium orthoaluminate crystals were prepared using standard melt growth processes [5, 21, 22, 34]. In undoped samples, used as references, the total concentration of paramagnetic impurities did not exceed 0.1 ppma.

As an example, this paper presents results for single crystals doped with Ti, V and Cr to  $(0.1–7) \times 10^{-2}$  at % according to chemical and spectral analysis data. The total concentration of other (unintentional) impurities was within  $\sim 1$  ppma as determined by spectral analysis. In crystals doped with rare-earth ions (Sm or Nd), the doping level was 50–100 ppma and the concentration of unintentional iron-group ions was  $\sim 1$  ppma. Samples for spectral and X-ray spectroscopic characterisation and determination of their stoichiometry and the electronic state of the host and impurity ions had the form of pellets 6–10 mm in diameter and 0.8–4 mm in thickness.

Some of the samples were given special thermal annealing, including multistep heat treatment, in oxidising ( $O_2$ ), reducing (CO, vacuum or  $H_2$ ) and neutral ( $H_2$ –Ar) atmospheres at  $T = 77, 600, 1400$  and  $1600$  K. Heat treatment of as-prepared samples and samples containing additional impurity ions (codoping) occasionally produces an additional absorption spectrum (AA). Some materials may have similar induced optical absorption (IA) and AA spectra.

Data for the samples studied are summarised in Tables 1–3. Note that the neodymium-doped strontium titanate samples had significant electrical conductivity and were thus difficult to characterise by EPR.

### 2.2. Spectroscopic techniques

Optical absorption and luminescence spectra were measured in the range 100–7500 nm ( $T = 77$  and  $300$  K) using Specord

M40 and M80, VM2, SDL1, SDL2 and DFS24 spectrophotometers. Cathodoluminescence spectra were obtained on a Zeiss Ultra A55 scanning electron microscope (SEM) using an HS101H digital camera ( $\lambda = 200–1100$  nm). Electron paramagnetic resonance (EPR) spectra were taken on a Varian spectrometer ( $\lambda = 0.8$  and  $3$  cm) at  $77$  and  $300$  K.

An atomic force microscope (AFM NP 206) and scanning electron microscopes (JEOL 840 and Zeiss Ultra A55) were used to examine the surface morphology of the samples before and after irradiation, plasma exposure or thermal annealing. The crystallographic parameters of the samples were determined on a DRON 3UM X-ray diffractometer at  $T = 80$  and  $300$  K.

### 2.3. Exposure to ionising and gamma radiation and plasma

The gamma dose in this study ( $^{60}Co$ ,  $E = 1.25$  MeV) was  $10^2$  to  $10^4$  Gy at  $T = 320$  K. A number of samples were electron-irradiated ( $E = 6$  MeV) at a beam density of  $\sim 10^{18}$  cm $^{-2}$  and  $T = 80$  and  $320$  K.

For plasma processing, we used two different plasma sources, which were described in detail elsewhere [36–38]. Note that both sources had the form of a plasma compressor with different beam densities (up to  $10^{22}$  cm $^{-2}$ ) and pulse durations (short and long pulses with  $\tau \sim 5 \times 10^{-6}$  and  $1.5 \times 10^{-4}$  s, respectively). The samples were exposed to a hydrogen or helium plasma with pulse energy densities from 5 to  $40$  J cm $^{-2}$ . The most likely temperature of the sample surface was estimated at  $T \approx 2300$  K, which was sufficient for surface modification. After the plasma processing, the thickness of the (polycrystalline) surface deformation layer was measured to be  $10^{-7}$  to  $10^{-6}$  m.

### 2.4. Local X-ray spectroscopy

X-ray line valence shift (XRLVS) measurements, a local method described in detail previously [4–6, 30], were used to assess the stability of the electronic state of the host and impurity ions in crystals upon changes in synthesis and/or irradiation conditions.

The stability of the valence state of the host and impurity ions in crystals and that of their stoichiometry were studied using a CAMEBAX X-ray microanalyser and double-crystal monochromator [15, 30].

The detection limit of the technique for the total impurity concentration (with appropriate corrections [39]) was  $\sim 1$  ppma, and that in electronic state stability evaluation was  $\sim 10$  ppma. The results varied from one point on the sample surface to another by 1% to 3%.

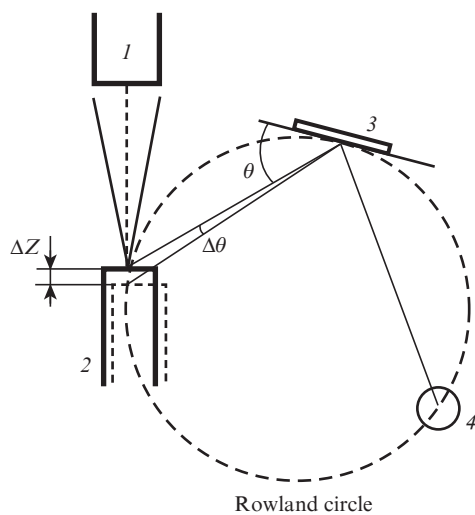
A simplified schematic of the X-ray microanalyser is presented in Fig. 1. An electron beam less than  $10^{-6}$  m in diameter, with an energy  $E \sim 10^4$  eV and current  $I = 10^{-10}$  to  $10^{-9}$  A, excites X-rays in the sample, which are dispersed by an analyser crystal and sent to a detector. To reduce experimental uncertainty, the signal is detected at each angle of the analyser crystal (1010 quartz). The X-ray line profile is well represented by a Lorentzian, and its peak position can be determined with an accuracy  $\varepsilon = \pm(60–130)$  meV.

The experimental technique used in the XRLVS measurements was analysed in detail elsewhere [5, 6, 28]. To experimentally determine the X-ray line shift ( $\Delta E_x$ ), we measured the change in the peak position of the  $K_{\alpha 1}$  lines of Ti, V, Cr, Sr and Nd ( $L_{\alpha 1}$  line) ions.

**Table 1.** Spectroscopic properties of sapphire crystals grown by various techniques.

Growth process	Absorption edge/nm	Centre wavelengths of absorption bands/nm	Centre wavelengths of IA bands/nm	TL peaks/nm	Relative TL intensity	Thermally stimulated conductivity peaks/K
V <sub>s</sub>	195	206*, 225*, 260*, 400*, 570	206, 225, 280, 475	690	0.01	388, 578
V <sub>p</sub>	142	175, 206, 230, 400*	206, 225, 280, 475*	320, 690	4	385, 560, 507
V <sub>sp</sub>	142	185*, 206*, 230*	–	420, 690	0.1	430, 507*, 560
DS <sub>s</sub>	145	175, 206*, 235*	206, 230	–	0.001	398*, 507*
DS <sub>r</sub>	142	175, 206, 235	206, 230, 280*, 470*	320, 420, 690	8	373, 506, 565
Cz <sub>r</sub>	143	180*, 206	206, 475	320, 420, 420, 690	2	430, 580
K <sub>r</sub>	142	198, 225*	–	–	0.001	387*, 426*, 485*
S <sub>r</sub>	142	175, 206, 230	206, 230	420	1	390, 418, 430, 506*

\* Weak bands.

**Figure 1.** Simplified schematic of the X-ray microanalyser: (1) electron gun, (2) sample, (3) analyser crystal, (4) detector.

### 3. Experimental results

The main spectroscopic properties of nominally undoped and doped sapphire, garnet and strontium titanate crystals are well known [1–4].

The short-wavelength fundamental absorption edge in sapphire references lies at  $\lambda = 142$  nm [1, 34], and that in YAG, at 152 nm [5, 27]. Perfect strontium titanate crystals are transparent in the range  $\lambda = 390$ –7500 nm [3].

#### 3.1. Effects of irradiation and heat treatment on the spectroscopic properties of crystals

**Sapphire.** Table 1 illustrates radiation-induced changes in the spectroscopic properties of sapphire crystals grown by the Verneuil process (V), Czochralski pulling (Cz), directional solidification (DS), the Kyropoulos method (K) and Stepanov method (S) from growth charges differing in quality: after standard (s), special (sp) and chemical (p) purification steps and recrystallisation (r). These data lead us to conclude that the sapphire crystals contain one type of colour centre, an F(V) centre [40, 41], i.e. an oxygen (cation) vacancy that captured an electron (hole), and that there are various concentrations of unintentional impurities. Clearly, the concentration and nature of colour centres depend on both the synthesis conditions and impurity composition of the material.

**Garnets.** The spectroscopic properties of undoped garnet crystals grown by the Czochralski technique, horizontal and

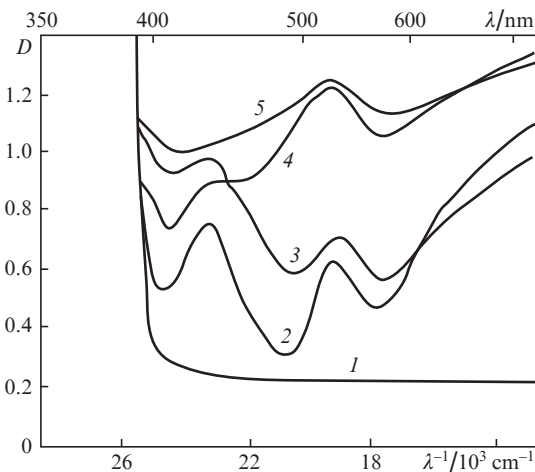
vertical directional solidification and other processes have been the subject of many studies (see e.g. Refs [1, 3, 5, 20, 29, 42, 43]).

After exposure to ionising radiation or high-energy electrons, the spectra of undoped yttrium aluminium garnet references, as well as those of other garnets, show a set of absorption (luminescence), thermoluminescence and thermally stimulated conductivity bands due to anion and cation vacancies that captured an electron or hole [21, 27]. Distinctions between trapping centres and their concentrations show up in thermally stimulated conductivity (TSC) and thermoluminescence (TL) spectra. As an example, Table 2 lists the TSC and TL peaks of YAG crystals heat-treated in vacuum and nitrogen. These data demonstrate that the annealing (preparation) procedure has a significant effect on the properties of the crystals [42, 43].

**Strontium titanate.** Perfect undoped SrTiO<sub>3</sub> crystals are transparent in the range 390–7500 nm. The absorption spectrum of such crystals is shown in Fig. 2 [spectrum (1)]. No luminescence bands were detected for perfect samples. The measured relative dielectric permittivity,  $\epsilon_0 = 365 \pm 5$  ( $v =$

**Table 2.** Temperature positions of thermoluminescence ( $T_{TL}$ ) and thermally stimulated conductivity ( $T_{TSC}$ ) peaks and activation energy for  $E$  trapping centres in YAG crystals heat-treated in vacuum and nitrogen.

Medium	Vacuum	Nitrogen
$T_{TL}/K$	425, 555	377, 420, 490, 547, 602
$T_{TSC}/K$	428, 560	380, 423, 495, 552, 607
$E/eV$	0.95, –	0.86, –, 1.05, 1.51, 2.1

**Figure 2.** Optical absorption spectra of SrTiO<sub>3</sub> crystals: (1) reference sample, (2) standard sample, (3) SrTiO<sub>3</sub>:Nd, (4) 'blue spot', (5) yellow region.

$10^3$  Hz), and refractive index,  $n = 2.4149$  ( $\lambda = 5.76 \times 10^{-7}$  m), of a reference sample with a density  $\rho = 5080 \text{ kg m}^{-3}$  and lattice parameter  $a = 3.9051 \times 10^{-10}$  m agree with earlier data [44–47]. A number of parameters of the samples, as well as data reported by different groups (see e.g. Refs [23, 35]) differ markedly. The main characteristics of the strontium titanate samples studied are listed in Table 3.

**Table 3.** Main spectroscopic characteristics of SrTiO<sub>3</sub> single crystals.

Crystal	at % impurity	$\epsilon$	Centre wave-length of absorption bands/nm	%Ti <sup>3+</sup>
SrTiO <sub>3</sub> (reference)	$10^{-5}$	360	–	–
SrTiO <sub>3</sub> (standard)	$(1 \pm 0.2) \times 10^{-3}$	$320 \pm 5$		$8 \pm 5$
SrTiO <sub>3</sub> ('blue spot')	$(1 \pm 0.2) \times 10^{-3}$	$120 \pm 5$	430, 520, 620	$22 \pm 6$
SrTiO <sub>3</sub> (yellow region)	$(1 \pm 0.2) \times 10^{-3}$	$220 \pm 5$	520, 620	$10 \pm 5$
SrTiO <sub>3</sub> :V	$(3 \pm 0.1) \times 10^{-2}$	$200 \pm 5$	620	$10 \pm 5$
SrTiO <sub>3</sub> :Cr	$(4 \pm 0.1) \times 10^{-2}$	$220 \pm 5$	–	$8 \pm 5$
SrTiO <sub>3</sub> :Ni	$(3 \pm 0.1) \times 10^{-2}$	$220 \pm 5$	–	$15 \pm 5$
SrTiO <sub>3</sub> :Pr	$(1 \pm 0.2) \times 10^{-2}$	$200 \pm 5$	430, 520, 620	$20 \pm 6$
SrTiO <sub>3</sub> :Sm	$(1 \pm 0.2) \times 10^{-2}$	$200 \pm 5$	520, 620	$20 \pm 6$
SrTiO <sub>3</sub> :Nd	$(1 \pm 0.2) \times 10^{-2}$	$150 \pm 5$	430, 520, 620	$28 \pm 6$

No induced absorption spectra were obtained after exposure of the strontium titanate references to any type of ionising radiation.

A number of samples, so-called boules, grown at a high rate comprised three regions: outer (transparent), intermediate (yellow) and inner ('blue spot') [4, 5]. The outer region had weak absorptions near 430 and 520 nm [Fig. 2, spectrum (2)], which were also observed in the neodymium-doped samples [spectrum (3)]. The inner region was easy to mechanically separate from the rest of the crystal and had strong absorption bands at  $\lambda = 430, 520$  and  $620$  nm [Fig. 2, spectrum (4)]. The intermediate region had absorption bands centred at  $520$  and  $620$  nm [Fig. 2, spectrum (5)].

Yttrium orthoaluminate, YAlO<sub>3</sub>, is similar in optical properties to YAG crystals and has strong absorption for  $\lambda > 190$  nm [48].

*Doped sapphire.* Titanium, vanadium and chromium ions in the crystal lattice of alumina substitute for Al<sup>3+</sup>, are coordinated by six oxygens in the form of a distorted octahedron (coordination number  $k = 6$ ) and have site symmetry  $C_3$  [3, 14].

The optical absorption spectrum of the sapphire crystals doped with Ti<sup>3+</sup> ( $3d^1$  electronic configuration) contains a strong absorption band near  $480$  nm and a broad band between  $700$  and  $1100$  nm, which are due to the  $3d(^2T) \rightarrow 4s(^2E)$  and  $3d \leftrightarrow 3d(^2T \rightarrow ^2E)$  transitions. Note that the strong UV absorption band of crystals doped with iron-group ions is often assigned to  $O^{2-} \rightarrow Me^{n+}$  charge transfer [1, 3].

The optical absorption spectrum of the  $\alpha$ -Al<sub>2</sub>O<sub>3</sub>:V<sup>3+</sup> crystals ( $3d^2$  configuration) comprises three strong bands, which are due to the  $^3T_1(t_2^2) \rightarrow ^3T_2(t_2e)$ ,  $^3T_1(t_2e)$  and  $^3A_2(e^2)$   $d \leftrightarrow d$  transitions and have maximum absorption coefficients at  $\lambda = 570, 400$  and  $323$  nm [3].

The optical absorption spectra of all the crystals doped with Cr<sup>3+</sup> ( $3d^3$  electronic configuration) contain three broad, strong bands (U, Y and V) in the visible and UV spectral regions, corresponding to the  $^4A_2(t_2^3) \rightarrow ^4T_2(t_2^2e)$ (U),  $^4T_1(t_2^2e)$ (Y)

and  $T_1(t_2e^2)$ (V) transitions (in the cubic crystal field approximation) at  $\lambda = 256, 405$  and  $555$  nm (ruby).

The trigonal distortion splits some of the energy levels [3]. In a number of sapphire and garnet crystals, the UV absorptions due to vibronic transitions are weak because of the strong absorption due to unintentional impurities. No such transition shows up in strontium titanate because of the fundamental absorption.

*Doped garnets.* The garnet ( $A_3B_2C_3O_{12}$ ) structure has three cation sites, which accommodate rare-earth ions (A site) and iron-group ions to form octahedral (B site) and tetrahedral (C site) centres.

The absorption spectrum of Ti<sup>3+</sup>-doped garnet crystals has two bands: a strong band around  $250$  nm, corresponding to the  $3d(^2T_2) \rightarrow 4s(^2E)$  transition, and a broad, weak band in the range  $500$ – $700$  nm, due to the  $^2D \rightarrow ^2E$  electronic transition of the  $3d$  Ti<sup>3+</sup> configuration in YAG. A similar band of multicomponent garnet crystals is shifted to the IR spectral region.

V<sup>3+</sup> ( $3d^2$  configuration) forms both octahedral and tetrahedral centres. For example, the optical absorption spectrum of Y<sub>3</sub>Al<sub>5</sub>O<sub>12</sub>:V<sup>3+</sup> crystals (Fig. 3) contains five bands, corresponding to transitions from the  $^3T_1(t_2^2)$  level to the  $^3T_2(t_2e)$ ,  $^3T_1(t_2e)$  and  $^3A_2(e^2)$  levels, with peak absorption wavelengths for the vanadium on the octahedral site  $\lambda = 425$  and  $625$  nm (YAG). The ground state for tetrahedral symmetry is  $^3A_2(e^2)$ . Absorption spectra are then determined by transitions from the  $^3A_2(e^2)$  level to the  $^3T$  (triplets) and  $^1A_1(e^2)$  (singlet) levels, with peak absorption wavelengths  $\lambda = 820$  and  $1280$  nm [43].

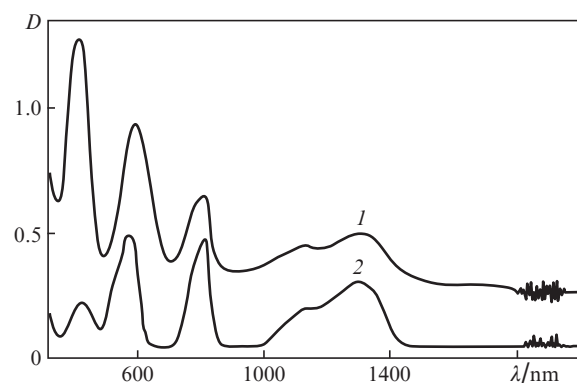


**Figure 3.** Absorption spectra of YAG:V crystals (1) before and (2) after annealing in an Ar–H<sub>2</sub> atmosphere.

It is known that, like other  $3d^3$  ions, Cr<sup>3+</sup> ions in garnet crystals form only octahedral centres [1, 3]. The two strong, broad bands (U and Y) in the visible and UV spectral regions [ $^4A_2(t_2^3) \rightarrow ^4T_2(^4T_1)$  transitions (in the cubic crystal field approximation)] are centred at  $\lambda = 588$  and  $431$  nm, and the V-band (YAG:Cr) peaks at  $268$  nm. A similar spectrum was reported for YAlO<sub>3</sub>:Cr [48].

An important feature of all the crystals and impurity ions under consideration is that the absorption, luminescence, thermoluminescence and thermally stimulated conductivity spectra of the doped sapphire and garnet crystals are free of the bands present in the spectra of the undoped crystals. This applies as well to chromium- and vanadium-doped yttrium orthoaluminate crystals [5, 21, 48].

*Exposure* of sapphire, ruby and garnet crystals, including yttrium orthoaluminate, with a doping level no higher than

$5 \times 10^{-2}$  at% to ionising radiation gives rise to strong IA bands and peaks, which differ from the absorption bands of their undoped counterparts (Tables 1–3).

Irradiation of the doped sapphire, garnet and yttrium orthoaluminate crystals to a gamma dose of  $10^4$  Gy or electron fluence of  $\sim 10^{19}$   $\text{cm}^{-2}$  increases the strength of the optical absorption bands due to  $\text{Ti}^{3+}$ ,  $\text{V}^{3+}$  or  $\text{Cr}^{3+}$  by 10% to 25%, depending on synthesis conditions. Note that the irradiation behaviour of the spectroscopic properties of strontium titanate has special features [21, 30].

The irradiation behaviour of the spectroscopic properties (IA spectra) of sapphire and, especially, garnet crystals is in a number of cases similar to that of samples that were given a special heat treatment and/or additionally doped with Ca (Mg) (so-called additional absorption spectra).

The IA and AA spectra of  $\text{YAG}:\text{V}^{3+}$  crystals show five absorption bands, centred at  $\lambda = 438, 590, 830, 1150$  and  $1300$  nm [Fig. 3, spectrum (2)]. Similar IA spectra were obtained for other vanadium-doped oxide crystals containing octahedral and tetrahedral cation sites [3].

After exposure to ionising radiation, the IA spectra of ruby and chromium-doped garnet crystals have four bands of different strengths, centred at 217, 270, 360 and 460 nm ( $\alpha\text{-Al}_2\text{O}_3:\text{Cr}$ ); 253, 282, 417 and 488 nm ( $\text{YAG}:\text{Cr}$ ); or 410, 505, 670 and 1050 nm ( $\text{GSAG}:\text{Cr}$  and  $\text{GSGG}:\text{Cr}$ ). It follows from these data that the IA spectra of the ruby and chromium-doped garnet-structure crystals consist of four absorption bands, which shift towards the IR spectral region with increasing lattice parameter. The spectra of the YAG and GSAG crystals codoped with Cr and Mg (Ca) ions (grown by vertical directional solidification) (Figs 4, 5) demonstrate that IA and AA may have different origins. Similar IA (AA) spectra were obtained for all the ruby and chromium-doped garnet crystals containing  $5 \times 10^{-3}$  to  $5 \times 10^{-2}$  at% chromium, independent of the preparation procedure.

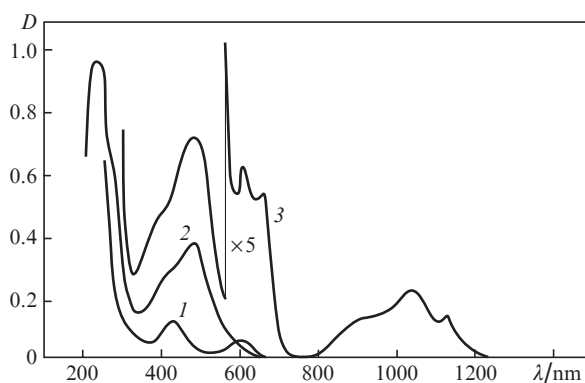


**Figure 4.** Optical absorption spectra of  $\text{YAG}:\text{Cr}:\text{Mg}$  crystals: (1) unannealed crystal, (2) IA, (3) AA after heat treatment ( $T = 1400$  K,  $\tau = 2.88 \times 10^4$  s).

Additional doping of garnet ( $\text{YAG}$ ,  $\text{GSGG}$ ,  $\text{GGG}$  and  $\text{YAIO}_3$ ) crystals with Mg or Ca may produce no changes in their absorption spectra but has a significant effect on the irradiation behaviour of their spectroscopic properties. Figures 4 and 5 illustrate the effects of gamma irradiation and thermal annealing on the optical absorption spectra of samples additionally doped with magnesium ions ( $\text{YAG}:\text{Cr}:\text{Mg}$ ) and  $\text{YAG}:\text{Cr}$  samples. Spectrum (1) in Fig. 4 shows typical strong UV and visible absorption bands of octahedral  $\text{Cr}^{3+}$  ions in

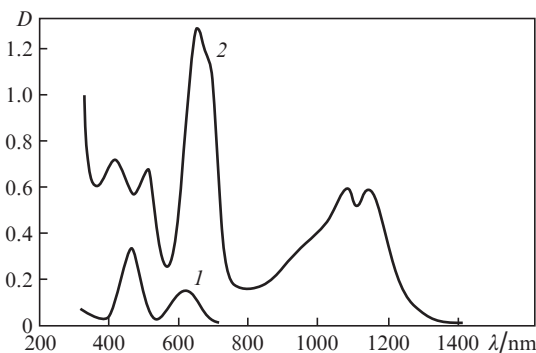


**Figure 5.** Optical absorption spectra of  $\text{GSAG}:\text{Cr}:\text{Ca}$  crystals: (1) unannealed crystal, (2) AA after heat treatment ( $T = 1400$  K,  $\tau = 2.88 \times 10^4$  s).

garnet crystals before irradiation or heat treatment [8, 43]. After high-temperature oxidising annealing, the  $\text{YAG}:\text{Cr}:\text{Mg}$  samples had IA bands centred at 253, 282, 417 and 488 nm [Fig. 4, spectrum (2)], similar to the IA bands of  $\text{YAG}:\text{Cr}$  crystals after exposure to ionising radiation. After high-temperature annealing, the AA spectrum contained additional bands centred at 640, 965 and 1100 nm ( $\text{YAG}:\text{Cr}:\text{Mg}$ ) or 505, 600 and 1055 nm ( $\text{GSGG}:\text{Cr}:\text{Ca}$ ). Similar behaviour was reported for  $\text{YAIO}_3:\text{Cr}:\text{Ca}$  [48].

The variation of the strength of IA bands with doping level (primarily with  $\text{Cr}^{3+}$  concentration) for crystals irradiated to various gamma doses and electron fluences was studied in detail [5, 43] and was shown to be nonlinear. Such behaviour is observed in EPR spectra, sensitive to  $\text{Cr}^{3+}$  concentration. One example is shown in Fig. 6. The  $-1/2 \leftrightarrow 1/2$  EPR signal intensity is a linear function of  $\text{Cr}^{3+}$  concentration, and its variation can be used to assess the irradiation-induced change in the valence state of some chromium ions in relation to the doping level and radiation dose. It follows from Fig. 6 that the percentage of  $\text{Cr}^{3+}$  varies most rapidly at low doping levels and high gamma doses [curve (3)]. Analysis of IA spectra indicates that the IA bands of both sapphire and the garnets are very weak, if any, below  $10^{-3}$  at%  $\text{Cr}^{3+}$  and above  $2 \times 10^{-1}$  at%  $\text{Cr}^{3+}$ , and are strongest at doping levels in the order of  $10^{-2}$  at%. The substantially nonlinear variation of the  $1/2 \leftrightarrow -1/2$  EPR

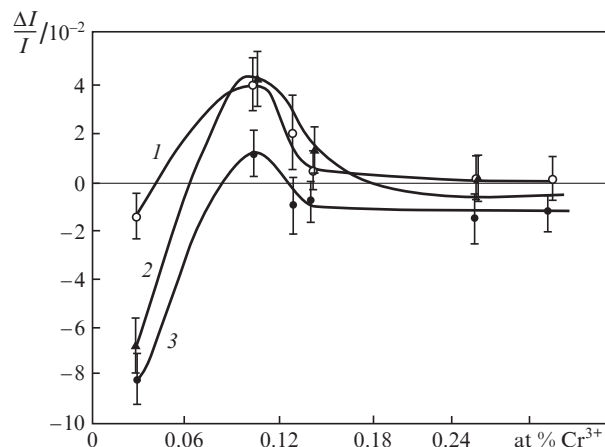


**Figure 6.** EPR signal intensity as a function of doping level for the  $\text{Cr}^{3+} -1/2 \leftrightarrow 1/2$  transition in  $\text{YAG}:\text{Cr}$  irradiated to a gamma dose of (1)  $10^2$ , (2)  $10^3$  and (3)  $10^4$  Gy.

signal intensity with chromium concentration and radiation dose can be interpreted as evidence for two-step or multistep dissociation of radiation-induced defects in garnet crystals. Similar data were obtained for  $\text{YAlO}_3:\text{Cr}$ , where radiation-induced defects are eliminated more rapidly than those in  $\text{YAG}:\text{Cr}$  [48].

Heat treatment of the irradiated ruby and garnet samples in air at  $T = 900$  K for 600 s eliminates all the IA bands and causes the EPR signal intensity and width to return to their original levels.

Note that such heat treatments under reducing conditions (vacuum or hydrogen) at  $T \geq 600$  K always considerably reduce or completely eliminate the AA bands of all the sapphire and garnet crystals studied [42].

**Doped strontium titanate.** Absorption spectra of strontium titanate crystals doped with iron-group ions have been studied in sufficient detail [3]. In this study, spectra of crystals doped with V, Cr, Mn and Co ions were measured at  $T = 4.2$  and 77 K. From characteristic absorption and EPR spectra, the valence state of the dopants was determined to be  $\text{Me}^{3+}$  (except for the manganese ions, a small part of which were in the  $\text{Mn}^{4+}$  state) [30, 45].

A weak impurity absorption in rare-earth-doped strontium titanate is only observed at low temperatures. Strong, broad absorption bands at  $\lambda = 430$  and 520 nm and a weak absorption at  $\lambda \sim 620$  nm are characteristic of  $\text{Nd}^{3+}$  and  $\text{Tm}^{3+}$  impurities. The corresponding optical absorption bands of  $\text{Sm}^{2+}$ -doped samples were observed at  $\lambda = 520$  and 620 nm.

Exposure of standard and doped samples to ionising radiation produces absorption bands or increases the strength of already existing bands at  $\lambda = 430$ , 520 and 620 nm by 6% to 8%. Heating to  $T = 400$  K in air rapidly eliminates the absorption bands.

Luminescence spectra were obtained for ‘blue spot’ and  $\text{SrTiO}_3:\text{V}$  (Cr, Mn, Co) samples before and after low-temperature treatment at  $T = 77$  K for 600 s. Earlier [46, 47],  $\text{SrTiO}_3:\text{Mn}$  samples that were given multistep heat treatment were shown to have a temperature anomaly. Cooling to  $T = 77$  K over a period of 60 s was accompanied by the development of a standard EPR spectrum of  $\text{Mn}^{4+}$  in a trigonal local environment. The spectrum persisted during subsequent heating to room temperature and then at  $T = 300$  K for several hours. The EPR spectrum of impurity ions in a cubic local environment emerged after the sample had been held at  $T = 600$  K for 600 s.

Note that, according to previous studies [49, 50], these samples showed significant dichroism around 700 nm and a small rise in absorption dispersion near 620 nm.

### 3.2. Scanning electron and atomic force microscopy results

Ionising radiation is known to produce no qualitative changes on the surface of oxide materials [5, 21]. The first studies concerned with the effect of high-energy plasma on the surface of strontium titanate crystals [51, 52] indicated the formation of single crystallites  $10^{-9}$  to  $10^{-7}$  m in size or arrays of such crystallites.

Figures 7 and 8 present some of the most interesting results obtained in studies of the surface of sapphire, ruby, yttrium aluminium garnet and strontium titanate after exposure to plasma flows.

Figure 7 shows surface SEM images of a reference strontium titanate sample and neodymium-doped sample (Fig. 7b) after plasma exposure. SEM images of other doped strontium

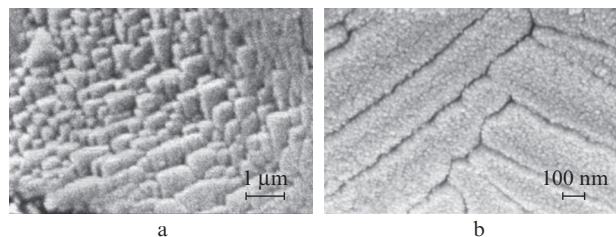


**Figure 7.** SEM images of the surface of  $\text{SrTiO}_3$  samples after plasma exposure of (a) a reference sample ( $W = 10 \text{ J cm}^{-2}$ ) and (b) neodymium-doped sample ( $W = 20 \text{ J cm}^{-2}$ ).

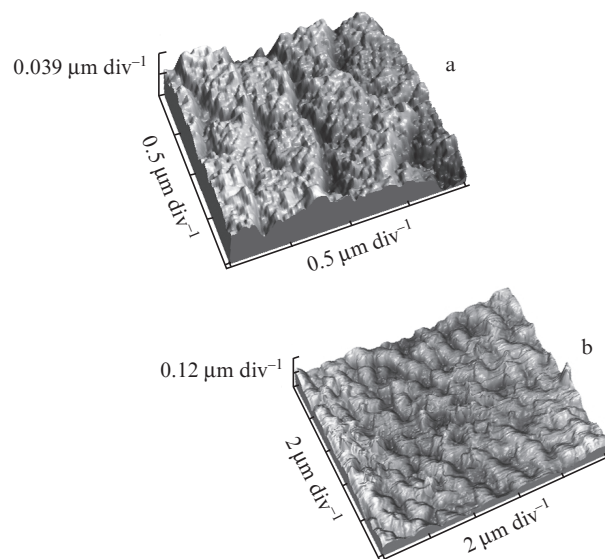


**Figure 8.** AFM images of the surface of (a)  $\text{SrTiO}_3$  and (b) ruby samples after plasma exposure to  $W = 10 \text{ J cm}^{-2}$ .

titanate samples after plasma exposure to a fluence of  $40 \text{ J cm}^{-2}$  were presented in previous reports [31–33, 51, 52].

Figure 8 shows AFM images of the surface of  $\text{SrTiO}_3:\text{Nd}$  and ruby crystals after plasma exposure to  $W = 10 \text{ J cm}^{-2}$ . Similar images were obtained for  $\text{YAG}:\text{Ce}$  crystals. The number density of crystallites on the garnet surface after plasma exposure to  $W = 10 \text{ J cm}^{-2}$  was five orders of magnitude lower than that on the strontium titanate and ruby crystals.

Preliminary analysis of SEM and AFM images indicated that plasma exposure resulted in the formation of a complex surface topography. On the surface of strontium titanate and ruby crystals, we observed the formation of ordered (or quasi-ordered) structures of single crystallites  $10^{-9}$  to  $10^{-7}$  m in size, which were, to a first approximation, pyramidal in shape.

### 3.3. X-ray spectroscopic investigation

The XRLVS method was used to assess the stability of the electronic state of impurity and host ions in crystals, in particular after gamma irradiation, thermal annealing or plasma exposure. The method builds on the dependence of the energy position of K, L and other characteristic X-ray lines on the electronic (valence) state of the ion. The X-ray lines considered in this study, e.g. those of the iron-group ions ( $\text{MeK}_{\alpha 1}$  lines), correspond to transitions between highly excited  $1s_{1/2}n^N$  and  $2p_{3/2}^5n^N$  configurations, which include core electrons (1s and 2p) and  $N$  outer (optical) 3d electrons. The energy corresponding

to an  $\text{MeK}_{\alpha 1}$  line is the energy difference between the  $\text{Me}^{n+}$   $1s_{1/2}n l^N$  and  $2p_{3/2}^5 n l^N$  states,

$$E_X^{n+} = E(2p_{3/2}^5 n l^N) - E(1s_{1/2}^5 n l^N), \quad (1)$$

and can be expressed through the valence of the  $\text{Me}^{n+}$  ion, directly related to the number of optical electrons,  $N$ .

For the iron-group ( $3d^N$  configuration) and lanthanoid ( $4f^N$  configuration) ions, a change in the number of optical electrons leads to a shift of their X-ray lines by about 1 eV [3–6, 39, 53]. The sign of the shift of the  $\text{MeK}_{\alpha 1}$  line profile shows unambiguously whether the valence of some of the ions decreases or increases, and the magnitude of the shift (valence shift) can be used to evaluate the relative and absolute concentrations of the ions involved.

The magnitude of the XRLVS is the energy difference between the  $\text{Me}^{n+}$  and  $\text{Me}^{n\pm 1}$  states [4, 6]:

$$\Delta E_X = E_X^{n+} - E_X^{n\pm 1}. \quad (2)$$

That the valence of iron-group or lanthanoid ions can be adequately determined using an X-ray microanalyser was demonstrated by comparing the measured chemical shift of the  $\text{TmL}_{\alpha 1}$  and  $\text{YbL}_{\alpha 1}$  lines of rare-earth fluorides to the valence shift of their  $\text{K}_{\alpha 1}$  lines obtained with a high-resolution spectrometer [53, 54].

The XRLVS method was used to assess the stability of the electronic state of the chromium ions in ruby under irradiation at doping levels from  $5 \times 10^{-2}$  to 0.86 wt %. The results of such measurements on a ruby sample containing  $(0.08\text{--}0.11) \times 0.02$  wt % chromium ions before and after gamma irradiation to a dose of  $10^4$  Gy are presented in Fig. 9. The irradiation shifted the  $\text{CrK}_{\alpha 1}$  line of the ruby to lower energies by  $\Delta E = -(0.56 \pm 0.13)$  eV. Similar results, with slightly lower  $\Delta E$  values, were obtained for other samples, containing up to  $\sim 2 \times 10^{-1}$  wt % ions.

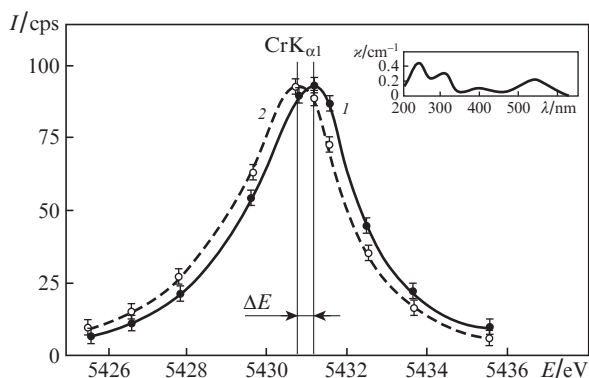


**Figure 9.**  $\text{CrK}_{\alpha 1}$  line profile (1) before and (2) after gamma irradiation of ruby (YAG) to a dose of  $10^4$  Gy. Inset: IA spectrum of ruby.

Despite the well-known effect of high-temperature heat treatment on the efficiency of radiation-induced defect formation in ruby and garnets, our experiments showed that the shift of the  $\text{CrK}_{\alpha 1}$  line depended little on heat treatment conditions. The  $\text{CrK}_{\alpha 1}$  lines obtained before and after irradiation of chromium-doped garnet crystals had similar profiles. Such results were obtained for various chromium-doped garnet crystals [8, 42]. YAG, GSGG and GSAG crystals doped with roughly the same concentration of chromium

ions had similar shifts (within experimental uncertainty) of the  $\text{CrK}_{\alpha 1}$  line.

The relative chromium ion concentration  $C_{\text{Cr}^{4+}}$  can be found as

$$C_{\text{Me}^{n\pm 1}} = (\Delta E_X^{\text{exp}} / \Delta E_X^{\text{theor}}) \times 100\%, \quad (3)$$

where  $\Delta E_X^{\text{exp}}$  and  $\Delta E_X^{\text{theor}}$  are the measured and calculated XRLVS values. The highest  $\text{Cr}^{4+}$  concentration is 9% to 25% (with a  $\pm 7\%$  uncertainty), depending on the doping level and ruby (garnet) preparation procedure. Irradiation reduces the  $\text{Cr}^{3+} 1/2 \leftrightarrow -1/2$  EPR signal intensity in ruby by 15% to 20%. X-ray spectroscopy data are consistent with EPR results. Note that heat treatment of gamma-irradiated ruby at  $T = 900$  K for 600 s eliminates its IA spectrum and reduces the EPR signal intensity to its original level. In addition, the  $\text{CrK}_{\alpha 1}$  line of the ruby returns to its original position. A shift of the  $\text{CrK}_{\alpha 1}$  line was also observed in garnet and yttrium orthoaluminate crystals doped with chromium to  $\sim (5\text{--}8) \times 10^{-2}$  at %.

In studies of radiation-induced defects in  $\text{SrTiO}_3:\text{Cr}(\text{V})$  crystals, no changes in their absorption or EPR spectra were detected, suggesting that the electronic state of the dopants in perfect crystals was rather stable. At the same time, as mentioned above, heat treatment produces strong optical absorption lines unrelated to impurity ions. Studies of such samples showed that the peak position of the  $\text{TiK}_{\alpha 1}$  line depended on the type of crystal. Figure 10 shows the  $\text{TiK}_{\alpha 1}$  line profiles for the strontium titanate samples studied. It is seen that the intensity of the  $\text{TiK}_{\alpha 1}$  line varies from sample to sample and that the line shifts to higher energies. Note that the intensity of the  $\text{SrK}_{\alpha 1}$  line varies within 2% to 5%, whereas its position remains unchanged to within experimental uncertainty.

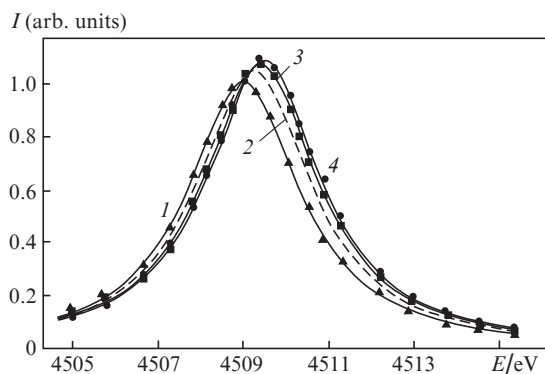


**Figure 10.**  $\text{TiK}_{\alpha 1}$  line profiles for strontium titanate: (1) reference sample, (2)  $\text{SrTiO}_3:\text{Mn}$ , (3, 4)  $\text{SrTiO}_3:\text{Nd}$  before and after plasma exposure, respectively.

To obtain theoretical values of  $E_X^{n+}$  and  $\Delta E_X$ , we used an *ab initio* method for calculations of the electronic structure of clusters [4–6, 53, 54], which will be considered in the next section.

The calculated valence shifts of the  $\text{TiK}_{\alpha 1}$  line for  $\text{SrTiO}_3:\text{Ni}$  and  $\text{SrTiO}_3:\text{Nd}$  relative to a reference are as follows:  $\Delta E(\text{TiK}_{\alpha 1}) = 0.32 \pm 0.09$  eV for  $\text{SrTiO}_3:\text{Ni}$  and  $\text{SrTiO}_3:\text{Sm}$ ;  $\Delta E(\text{TiK}_{\alpha 1}) = 0.50 \pm 0.09$  eV for  $\text{SrTiO}_3:\text{Nd}$  before plasma exposure and  $0.62 \pm 0.09$  eV after.

The fraction of  $\text{Ti}^{3+}$  estimated by Eqn (3) is  $18 \pm 6\%$  in  $\text{SrTiO}_3:\text{Ni}$  and  $28 \pm 6\%$  in  $\text{SrTiO}_3:\text{Nd}$  (Table 3). The intensity ratio of the  $\text{TiK}_{\alpha 1}$  and  $\text{SrK}_{\alpha 1}$  lines is unity in a reference mate-

rial and 1.0 and 1.33 in the samples studied. Note that plasma exposure further increases the intensity of the  $\text{TiK}_{\alpha 1}$  line on the surface of strontium titanate.

The position of the  $L_{\alpha 1}$  line of rare-earth dopants in garnet, strontium titanate, and yttrium orthoaluminate crystals remained unchanged to within the accuracy in our measurements.

#### 4. Theoretical calculation results

To more accurately identify the optical absorption spectra and shifts of characteristic X-ray lines of doped sapphire, garnet, yttrium orthoaluminate and strontium titanate crystals, we performed *ab initio* self-consistent field calculations of the energies corresponding to X-ray lines and  $3d \leftrightarrow 3d$  ( $4s \leftrightarrow 3d$ ) transitions of metal ions in clusters. Particular attention was paid to  $\text{Ti}^{n+}$ ,  $\text{V}^{n+}$  and  $\text{Cr}^{n+}$  ions in  $\text{Me}^{n+}:[\text{O}^{2-}]_k$  clusters. The impurity ion in such a cluster is coordinated by  $k$  ligands (e.g. oxygen ions). The symmetry of the cluster corresponds to that of the nearest neighbour environment of the impurity ion in the crystal lattice [4–6].

Theoretical analysis of the structure of a cluster composed of an impurity ion and ligand ions and necessary calculations can be performed in a substantially simplified model [6]. Using the one-electron approximation, central field functions and a normalised antisymmetric set of one-electron wave functions for cluster ions, the cluster energy can be written in the form [25, 28, 33]

$$E(\text{Me}^{n+}:[\text{L}]_k) = E_0 + kE_1 + k'(E_Z + E_c + E_{\text{ex}}), \quad (4)$$

where  $E_0$  ( $E_1$ ) is the total energy of the impurity ion (ligand) in a free state, and  $E_Z$ ,  $E_c$  and  $E_{\text{ex}}$  represent the interactions between the ions and electrons in the cluster. Exact expressions for  $E_Z$ ,  $E_c$  and  $E_{\text{ex}}$  in Eqn (4) can be found in Refs [6, 55]. Minimising (4) with respect to the radial parts of the wave functions (orbitals) of the ions in the system, we can obtain a system of self-consistent field equations for a cluster, similar to the Hartree–Fock equations [56] for a free ion. The expressions derived in Refs [6, 55–57] for the Coulombic [ $Y'(\text{nl}|r)$ ] and exchange [ $X'(\text{nl}|r)$ ] potentials differ from the corresponding Hartree–Fock potentials by additional terms that represent the interaction between the ions in the cluster.

As shown earlier [4–6], solutions to the system of self-consistent equations for a cluster are determined, among other things, by boundary conditions set for a free (single) cluster in the form  $P(\text{nl}|r)|_{r \rightarrow \infty} \rightarrow 0$  or in the form of Wigner–Seitz conditions:  $(\partial P(\text{nl}|r)/\partial r)|_{r \rightarrow r_0} \rightarrow 0$ . The dependence of radial integrals on the type of boundary condition and the parameter  $r_0$  in Wigner–Seitz conditions was analysed in detail in Refs [4–6, 57–59].

The final expression for the energy of the Stark components of the  $\text{Me}^{n+}$  ion in a cluster (crystal) can be written in the form

$$E(\text{nl}^N|\alpha\alpha'\text{LSJ}) = E'_0 + \sum_i e_i(l^N, \alpha\alpha'\text{LS}) E_i(\text{nl}, \text{nl}) + \chi(\text{LSL}'S', \text{J})\eta(\text{nl}) + \sum_{k,q,i} B_{kq} Y_{kq}(\Theta_i \Phi_i), \quad (5)$$

where  $E'_0$  is the centre-of-gravity energy of the  $\text{nl}^N$  configuration of the  $\text{Me}^{n+}$  ion in the cluster;  $\eta(\text{nl})$  is the spin–orbit

coupling constant; and  $E_i(\text{nl}, \text{nl})$  are the radial Racah integrals ( $B$  and  $C$  integrals for the iron-group ions), which can be written as linear combinations of Slater integrals [56]. Classic expressions for the angular coefficients in the Coulomb energy [ $e_i(l^N, \alpha\alpha'\text{LS})$ ] and spin–orbit interaction energy [ $\chi(\text{LSL}'S', \text{J})$ ] and for the Stark splitting  $B_{kq}$  ( $Dq$  for metal ions [ $Y_{kq}(\Theta_i \Phi_i)$  are spherical harmonics]) can be found in Refs [3, 59].

The system of Hartree–Fock–Pauli equations used by us for clusters and the corresponding computation programs take into account the influence of main relativistic effects [59] and allow one to adequately determine changes in the radial part of one-electron orbitals in going from a free ion to a crystal and from one crystal to another, which is completely ignored in crystal field theory. The changes in radial Racah (Slater) integrals and their dependences on the nature of ligands and lattice parameter (nephelauxetic effect) computed using programs described earlier [4–6] agree sufficiently well with experimental data [33, 58].

Numerical calculations indicate that, when a free  $\text{Me}^{n+}$  ion is incorporated into a cluster, its total energy decreases by 0.2–0.5 a.u. (by 0.3–0.6 a.u. for the rare-earth ions). For example, the total energy of the  $\text{Cr}^{3+}$  ion changes from  $E_0(\text{Cr}^{3+})^{\text{free}} = -1047.7132$  a.u. to  $E_0(\text{Cr}^{3+})^{\text{clust}} = -1047.1939$  a.u. In addition, the  $F^2(3d, 3d)$  integrals for the  $\text{Cr}^{3+}$  ion decrease from 87080 to 72010  $\text{cm}^{-1}$ , in good agreement with experimental data [3]. Note that the theoretical data obtained in this approximation for both the iron-group ions and lanthanum and actinium ions coordinated by various ligands (fluorine, oxygen and chlorine ions) agree sufficiently well with experimental data [3, 14].

For a titanium ion in possible  $\text{Ti}^{3+}:[\text{O}^{2-}]_k$  clusters with  $R_{\text{Ti-O}}$  distances from 2.2 to 1.8 Å and  $k = 4$ –6 for octa- and tetragonal sites, the theoretical value of  $Dq$  ranges from 1930 (strontium titanate,  $k = 6$ ) to 1400  $\text{cm}^{-1}$  (sapphire,  $k = 6$ ; strontium titanate,  $k = 4$ ).

To evaluate the energy of the  $\text{Ti}^{3+}$   $3d \rightarrow 4s$  transition, we calculated the electronic structure of a cluster for two  $\text{Cr}^{3+}$  configurations ( $[\text{Ar}]3d$  and  $[\text{Ar}]4s$ ), with  $R_{\text{Ti-O}}$  increased by 0.1 Å for the excited configuration. The calculated energy of the  $\text{Ti}^{3+}$   $3d_{5/2} \rightarrow 4s_{1/2}$  electronic transition, allowed owing to the noncentral crystal field component, is 2.8 eV, which corresponds to an absorption band at 425 nm. The  $3d \leftrightarrow 3d$  transitions between the Stark levels of the  $[\text{Ar}]3d$  configuration are represented by a broad band with a peak absorption wavelength  $\lambda = 610$  nm.

As mentioned above, the optical absorption spectrum of  $\text{YAG}:\text{V}^{3+}$  contains five bands, corresponding to the  ${}^3\text{T}_1(\text{t}_2^2) \rightarrow {}^3\text{T}_2(\text{t}_2\text{e})$ ,  ${}^3\text{T}_1(\text{t}_2\text{e})$  and  ${}^3\text{A}_2(\text{e}^2)$  transitions, with peak absorption wavelengths of 425 and 625 nm for vanadium on the octahedral site and 820 and 1280 nm for vanadium on the tetrahedral site. Calculation of the radial integrals for  $\text{V}^{3+}:[\text{O}^{2-}]_k$  clusters with  $k = 6$  and 4 yields parameters approaching semiempirical values:  $Dq = 1780$   $\text{cm}^{-1}$  and  $B = 740$   $\text{cm}^{-1}$  for octahedra and  $Dq = 820$   $\text{cm}^{-1}$ ,  $B = 480$   $\text{cm}^{-1}$  and  $C = 2600$   $\text{cm}^{-1}$  for tetrahedra. The IA bands at 650 and 730 nm produced by irradiation of vanadium-doped garnet crystals are due to transitions of  $\text{V}^{4+}$  ions in octahedral and tetrahedral environments.

As an example, Tables 4–6 present calculation results for the radial integrals and energy of  $\text{Cr}^{n+}$  levels in  $\text{Cr}^{n+}:[\text{O}^{2-}]_k$  clusters ( $n = 3, 4$ ;  $k = 6, 4$ ;  $R = 1.5$ –2.1 Å). Test calculations of the radial integrals and energy of chromium ions in various coordinations and at various interionic distances fit well with the absorption spectra of  $\text{Cr}^{3+}$  in garnet, ruby, perovskites

**Table 4.** Semiempirical and theoretical values of  $B$ ,  $C$  and  $Dq$  for  $\text{Cr}^{3+}$  ions in various crystals.

Crystal	$B/\text{cm}^{-1}$	$C/\text{cm}^{-1}$	$Dq/\text{cm}^{-1}$
$\alpha\text{-Al}_2\text{O}_3$	682	3120	1787
$\text{Y}_3\text{Al}_5\text{O}_{12}$	725	3373	1650
$\text{Gd}_3\text{Sc}_5\text{O}_{12}$	740	3578	1500
$\text{Gd}_3\text{Sc}_2\text{Ga}_3\text{O}_{12}$	740	3578	1500
$\text{SrTiO}_3$	690	3210	1760
$\text{Cr}^{3+}:\text{[O}^{2-}]_6$ ( $R = 2.0 \text{ \AA}$ )	789	2829	1750

**Table 5.** Theoretical energies of  $\text{Cr}^{4+}$  levels (octahedral site) in YAG and GSGG crystals doped with chromium and calcium (magnesium).

Level	YAG:Cr			GSGG:Cr		
	$\Delta E/\text{cm}^{-1}$	$\lambda_{\text{max}}^{\text{theor}}/\text{nm}$	$\lambda_{\text{max}}^{\text{exp}}/\text{nm}$	$\Delta E/\text{cm}^{-1}$	$\lambda_{\text{max}}^{\text{theor}}/\text{nm}$	$\lambda_{\text{max}}^{\text{exp}}/\text{nm}$
${}^3\text{T}_1$	0	–	–	0	–	–
${}^1\text{T}_2$	12549	797	–	12334	810	–
${}^1\text{E}$	12737	785	–	12551	797	–
${}^3\text{T}_2$	20815	480	480	19318	517	520
${}^1\text{A}_1$	27332	365	380	26775	373	400
${}^3\text{T}_1$	31581	316	290	36536	327	300
${}^1\text{T}_2$	34968	285	–	33337	300	–
${}^1\text{T}_1$	37913	263	260	36346	275	268
${}^3\text{A}_2$	43315	230	231	40318	248	250

**Table 6.** Theoretical and experimental wavelengths corresponding to  $d \leftrightarrow d$  transitions of the  $\text{Cr}^{4+}:\text{[O}^{2-}]_4$  cluster in YAG and GSGG crystals.

Level	$\text{Y}_3\text{Al}_5\text{O}_{12}$		$\text{Gd}_3\text{Sc}_2\text{Ga}_3\text{O}_{12}$	
	$\lambda^{\text{theor}}/\text{nm}$	$\lambda^{\text{exp}}/\text{nm}$	$\lambda^{\text{theor}}/\text{nm}$	$\lambda^{\text{exp}}/\text{nm}$
${}^3\text{A}_2$	–	–	–	–
${}^1\text{E}$	10950	11000	847	–
${}^3\text{T}_2$	964	964	1052	1052
${}^3\text{T}_1$	640	640	661	600
${}^1\text{A}_1$	627	–	507	504
${}^1\text{T}_2$	517	–	475	504
${}^1\text{T}_1$	453	–	407	410
${}^3\text{T}_1$	410	–	410	410

and other oxides (Table 4). The calculated energy levels of  $\text{Cr}^{4+}$  in  $\text{Cr}^{4+}:\text{[O}^{2-}]_{4,6}$  clusters are consistent with the IA and AA spectra of ruby, garnet and perovskite crystals (Tables 5, 6). Comparison of the calculated and measured spectra of oxide crystals doped with iron-group ions demonstrates that the spectra are in good quantitative agreement and that the experimental data can be adequately interpreted.

In semiempirical calculations of spectra of  $3d^2$  ions ( $\text{Cr}^{4+}$  and  $\text{V}^{3+}$ ) in octahedral and tetrahedral environments, the parameter  $Dq$  corresponds to the energy separation between the  ${}^3\text{A}_2$  and  ${}^3\text{T}_2$  levels. An experimental value of  $Dq$  was evaluated from the separation between the peak positions (centroids) of the bands corresponding to these transitions in YAG and GSAG crystals. In this way, we obtained the following values:  $Dq_{\text{oct}} = 2250 \text{ cm}^{-1}$ ,  $Dq_{\text{tet}} = 1033 \text{ cm}^{-1}$  and  $Dq_{\text{oct}} = 2100 \text{ cm}^{-1}$ ,  $Dq_{\text{tet}} = 950 \text{ cm}^{-1}$ . To estimate the Racah parameter  $B$  for  $\text{Cr}^{4+}$  on the tetrahedral site, we used the 77-K additional absorption spectrum and assumed the two narrow bands around 1080 and 1116 nm to correspond to a transition from the  ${}^3\text{A}_2$  ground state to a split  ${}^1\text{E}$  state ( $A$  and  $B$ ). To a first approximation, the relative position of the  ${}^1\text{E}$  level is independent of  $Dq$ , and at  $C/B = 4$  the separation between the  ${}^1\text{E}$  and  ${}^3\text{A}_2$  levels is  $\Delta E \approx 16 \text{ eV}$  [5], which gives  $B = 510 \text{ cm}^{-1}$ . In the other instances, we used a range of  $B$  values in semi-

empirical energy level calculations and found the result that was in the best agreement with measured band positions. Based on the self-consistent field theory for clusters, we calculated X-ray energies of ions in clusters. The X-ray energies thus found for titanium, vanadium and chromium ions were reported previously [60, 61]. Note that theoretical results agree sufficiently well with experimental data in Ref. [39]:  $E(\text{TiK}_{\alpha 1}) = 4511 \text{ eV}$ ,  $E(\text{VK}_{\alpha 1}) = 4952 \text{ eV}$  and  $E(\text{CrK}_{\alpha 1}) = 5415 \text{ eV}$ .

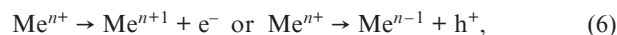
The calculated shift of X-ray lines in going from free iron-group and lanthanoid ions to crystals is rather small:  $\Delta E_X = 1\text{--}3 \text{ eV}$ . The X-ray line valence shift is, for example, 0.18 to 0.6 eV for the chromium ion (for  $\text{MeK}_{\alpha,\beta}$  lines).

## 5. Discussion

Spectroscopic studies of undoped alumina, garnet and strontium titanate crystals lead us to conclude that there is one set of point defects and colour centres in the oxide materials under consideration. These are, first of all, oxygen vacancies, including those that captured an electron (analogues of the F-centre in alkali halide crystals), and cation vacancies that captured holes (V-centres). Colour centres are responsible for the optical absorption bands in the range 160–230 nm, which disappear when the concentration of iron-group and/or lanthanoid ions exceeds 10 ppm. The other optical absorption bands in the crystals under consideration are due to impurities; i.e. the probability of charge formation and capture by structural defects in doped sapphire, garnet and yttrium orthoaluminate crystals decreases with increasing doping level.

In most of the strontium titanate samples studied, a major defect (colour centre) is the  $\text{Ti}^{3+}$  ion, whose formation is stimulated by the generation of oxygen vacancies in the crystal. Their concentration is many orders of magnitude higher than the dopant concentration, which nullifies the doping effect in the material.

The major colour centres in oxide crystals doped with iron-group ions to less than 0.1 at% are electron ( $e^-$ ) and/or hole ( $h^+$ ) centres due to changes in the electronic state of impurities in the region of higher or lower valences,



followed by electron or hole capture by an impurity cluster. This explains why alumina, garnets, yttrium orthoaluminate and strontium titanate have similar induced absorption spectra, which depend only on the nature and electronic structure of the activator.

The lighter iron-group ions (Ti, V and Cr) usually follow the left scheme in (6), with an increase in the effective charge of the dopant and the formation of an electronic trapping centre. In the case of the heavier iron-group ions (Co, Ni and Cu), a more likely process is the formation of a hole centre, accompanied by a decrease in the valence of the dopant [5, 6]. Changes in the electronic state of the host titanium ions in strontium titanate are determined by active formation of oxygen vacancies during the synthesis and heat treatment of the crystals.

This approach is consistent with the classic scheme of defect formation in crystals. The stability of the electronic state of an impurity can be assessed qualitatively and quantitatively by comparing the ionisation energies of a metal ion,

$I_{Me^{n+}}$ , with the Madelung constant,  $\alpha_M$ , for the corresponding cation site of the crystal lattice [4–6]. All possible cases are described by the relation  $I_{Me^{n+}} < |\alpha_M| < I_{Me^{n\pm 1}}$ , which can be used to evaluate the possible electronic state of the dopant on any lattice (interstitial) site.

For example, according to Bartram et al. [40]  $\alpha_M = -35.2$  eV for the cation site in an ideal sapphire crystal. A necessary condition for the electronic state of  $Me^{n+}$  to be stable is  $I_{Me^{n+1}} > |\alpha_M|$ . In an ideal crystal, impurity (Ti, V, or Cr) ions can only be present in the form of  $Me^{3+}$  ions because the relevant ionisation potentials are  $I_{Me^{3+,4+}}$  (eV) = 27.49, 43.27 (Ti), 29.31, 46.71 (V), 30.96 and 46.71 (Cr). When an electron resulting from dopant ionisation is localised in the second coordination sphere of a cluster,  $\alpha_M$  increases by 5.5 eV, which changes the electronic state of the impurity if  $I_{Me^{n+}}$  and  $\alpha_M$  differ little. This is the case of titanium and chromium ions in irradiated sapphire (ruby) and garnet crystals. A detailed analysis should take into account the change in  $\alpha_M$  due to the difference in ionic radius between the dopant and host ions ( $Al^{3+}$ ,  $Sc^{3+}$  and others) and the change in the lattice sum (increase in  $\alpha_M$  by approximately 10%–15%) because of the decrease in the  $Me^{n+1}-O^{2-}$  interionic distance. With such corrections, we obtain  $|\alpha_M| \approx 45$  eV. The electrical double layer formed by the displaced ions in the first and second coordination spheres of the cluster stabilises the  $[Me^{n+1}:O^{2-}]_k + e^-$  cluster for the lighter iron-group ions. Heating of samples leads to thermal activation of an electron, which is then captured at an impurity ion.

X-ray spectroscopic studies of doped sapphire and garnet crystals [5, 21] indicated an effective transition of some (up to 20%) of the Ti, V, and Cr impurity ions from the trivalent to tetravalent state. The transition can be induced by gamma irradiation and synthesis or thermal annealing under oxidising conditions. In strontium titanate, which contains  $Ti^{4+}$  as a structural component, this ion may convert to  $Ti^{3+}$  ( $3d^1$  configuration) to compensate the charge of oxygen vacancies.

*Ab initio* simulation of the electronic structure of impurity clusters made it possible to obtain radial integrals and energies of levels and electron transitions in the optical and X-ray ranges that agreed with experimental data. The numerical calculation results fit sufficiently well with the observed optical spectra of doped crystals in the visible, IR and X-ray ranges both before and after heat treatment or irradiation of the crystals.

The optical absorption spectra of irradiated garnet crystals contain IA bands at  $\lambda \approx 232, 260, 290$  and 485 nm (YAG:Cr) or at  $\lambda \approx 270, 295, 400$  and 425 nm (mixed garnets). The latter bands are slightly shifted relative to the IA bands of ruby ( $\lambda \approx 217, 270, 360$  and 460 nm) and perovskite  $YAlO_3:Cr$  ( $\lambda \approx 295, 385, 425$  and 500 nm).

The IA spectra of irradiated ruby or chromium-doped garnets correspond to the energy of transitions of the impurity ions in  $Cr^{4+}:[O^{2-}]_k$  clusters with  $k = 6$  and 4 both before and after gamma irradiation. According to the shift of the  $CrK_{\alpha 1}$  line and calculated IA spectra, irradiation of chromium-doped sapphire, garnet, or yttrium orthoaluminate samples leads to conversion of some of the  $Cr^{3+}$  ions to  $Cr^{4+}$ , electron capture at a  $Cr^{4+}:[O^{2-}]_6$  cluster and the formation of a system similar to a localised exciton,  $Cr^{4+}:[O^{2-}]_6 + e^-$ . The resulting IA spectrum, composed of four bands, is due to transitions of the  $Cr^{4+}$  ions in the  $Cr^{4+}:[O^{2-}]_6$  cluster (three bands). The origin of the fourth band in the IA spectrum requires further investigation. It may be due to an electron transition in the

hydrogen-like system  $[Cr^{4+}:[O^{2-}]_6]^+ + e^-$  or to an impurity exciton. Heat treatment of the irradiated crystals at  $T = 600$  K for 600 s leads to thermal activation of an electron, which is then captured at a chromium ion ( $Cr^{4+} + e^- \rightarrow Cr^{3+*}$ ), resulting in emission of a photon.

A detailed analysis of the results indicates that the spectra of IA and AA (due to additional doping with Ca or Mg) in garnet samples correspond to transitions of  $Cr^{4+}$  ions in both octahedral and tetrahedral clusters. The presence of optical absorption bands of garnet crystals in the long-wavelength region of their spectrum suggests that there is a weak crystal field, which is characteristic of fields with tetrahedral symmetry:  $Dq_{tet} = \frac{4}{9}Dq_{oct}$ . Theoretical results and experimental data lead us to conclude that three IA and AA bands of these crystals are due to  $d \leftrightarrow d$  transitions in tetrahedral and octahedral  $Cr^{4+}:[O^{2-}]_k$  clusters.

The high strength of the IA bands due to  $d \leftrightarrow d$  transitions of impurity ions is the consequence of the increase in the charge of the  $Cr^{4+}$  ion core and partial ‘permission’ for  $3d \leftrightarrow 3d$  transitions because of the increase in the asymmetric crystal field component.

Note that the formation of  $Cr^{4+}$  ions in tetrahedral clusters is due not only to the increase in the valence of the dopant but also to the formation of clusters with a different coordination at sufficiently low temperatures ( $T \ll 1400$  K). This can be accounted for by the fact that the activation energy for the transition of a chromium ion from an octahedral to tetrahedral site is inversely related to the oxygen vacancy concentration in the crystal.

Table 4 presents theoretical and semiempirical values of the radial integrals for  $Cr^{3+}$  ions in various crystals, which are seen to be in rather good agreement. Tables 5 and 6 list theoretical and experimental values of the energies of  $Cr^{4+}$  levels in octahedral and tetrahedral clusters in garnet crystals, the experimentally determined peak absorption wavelengths ( $\lambda_{max}$ ) of octahedral  $Cr^{4+}$  ions in YAG and GSGG crystals codoped with Mg and Cr ions and the corresponding theoretical values obtained at  $Dq = 2250$   $cm^{-1}$ ,  $B = 830$   $cm^{-1}$  and  $C = 3569$   $cm^{-1}$  for YAG and  $Dq = 2100$   $cm^{-1}$ ,  $B = 860$   $cm^{-1}$  and  $C = 3354$   $cm^{-1}$  for GSGG. As seen in Table 5, the calculated and observed peak positions of the main transitions  ${}^3T_1 \rightarrow {}^3T_2$ ,  ${}^3A_2$ ,  ${}^3T_1(P)$  are in good agreement. At the same time, reliable agreement between the positions of the bands observed in the ranges 380–400 and 260–270 nm, due to transitions to the  ${}^1A_1$  and  ${}^1T_1$  levels, requires additional investigation, first of all with allowance for their strength. The following values of the radial integrals were obtained for  $Cr^{4+}$  ions in a tetrahedral cluster:  $Dq = 1037$   $cm^{-1}$ ,  $B = 590$   $cm^{-1}$  and  $C = 2301$   $cm^{-1}$  in YAG and  $Dq = 950$   $cm^{-1}$ ,  $B = 730$   $cm^{-1}$  and  $C = 3134$   $cm^{-1}$  in GSGG.

The AA spectrum of garnets additionally doped with Ca or Mg can also be obtained by oxidising annealing or exposure to ionising radiation. Czochralski-grown YAG:Cr:Mg and  $YAlO_3:Cr:Ca$  crystals had such a spectrum in the as-grown state. Like in the case of GSGG:Cr, oxidising annealing increased the strength of the absorption bands. Irradiation of mixed garnets (GSGG, YSGG and GSAG) produces an IA spectrum similar to that of gamma-irradiated YAG. The absorption bands of GSAG:Cr and GSGG:Cr are shifted to longer wavelengths relative to the spectrum of YAG:Cr and are centred at  $\lambda = 253, 282, 417$  and 488 nm in GSAG:Cr and at  $\lambda \approx 410, 505, 670$  and 1050 nm in GSGG:Cr. Note that, during annealing, the strengths of all the bands vary

in a similar manner, suggesting that they arise from the same centre.

Calculation of the radial integrals for  $V^{n+}:[O^{2-}]_k$  clusters with vanadium on octahedral and tetrahedral sites yielded values approaching semiempirical parameters:  $Dq = 1700 \text{ cm}^{-1}$  and  $B = 700 \text{ cm}^{-1}$  (octahedron) and  $Dq = 800 \text{ cm}^{-1}$ ,  $B = 480 \text{ cm}^{-1}$  and  $C = 2500 \text{ cm}^{-1}$  (tetrahedron). The IA bands near  $\lambda \approx 438$  and  $590 \text{ nm}$  produced by gamma irradiation of YAG:V are due to transitions of  $V^{3+}$  ions in an octahedral environment, and the bands centred near  $\lambda \approx 830$ ,  $1150$  and  $1300 \text{ nm}$  are due to tetrahedrally coordinated  $V^{3+}$ . The absorption bands of  $V^{4+}$  near  $300$  and  $750 \text{ nm}$  seem to overlap with the corresponding bands of octahedrally coordinated  $V^{3+}$ .

Theoretical and experimental studies of crystals doped with vanadium and chromium and containing Ca or Mg as a codopant demonstrate that  $Cr^{4+}$  or  $V^{3+}$  ions ( $3d^2$  electronic configuration) are incorporated into octahedral or tetrahedral sites of the garnet lattice. This refers not only to yttrium aluminium garnet but also to gadolinium scandium gallium, gadolinium scandium aluminium and yttrium scandium gallium garnets.

MeK $_{\alpha 1}$  XRLVS measurement results lend support to the conclusion that both irradiation and high-temperature oxidising annealing of sapphire and garnet crystals increase the valence of chromium, titanium and vanadium impurity ions.

In irradiated ruby and chromium-doped garnet and yttrium orthoaluminate crystals, the CrK $_{\alpha 1}$  line is shifted to lower energies, suggesting that some of the chromium ions converted from the  $Cr^{3+}$  state to  $Cr^{4+}$  (Fig. 9).

Data on the TiK $_{\alpha 1}$  X-ray lines of  $Ti^{n+}:[O^{2-}]_k$  clusters provide conclusive evidence that some of the  $Ti^{4+}$  ions in strontium titanate crystals convert to a trivalent state, which is the consequence of an increase in the concentrations of oxygen and strontium vacancies and deviations from stoichiometry (Fig. 10).  $Ti^{3+}$  ions may occupy not only the octahedral sites of the  $Ti^{4+}$  ions but also strontium sites ( $Ti_{Sr^{2+}}^{3+}$ ) and cation sites with an oxygen vacancy (oxygen vacancies) in the nearest neighbour environment of titanium ions. The different positions of titanium ions in the crystal lattice of strontium titanate can be represented by  $Ti^{n+}:[O^{2-}]_k$  clusters with  $k = 3-5$ .

Analysis of SEM and AFM images indicates that hydrogen and helium plasma exposure of sapphire, yttrium aluminium garnet and strontium titanate single crystals produces a polycrystalline layer  $10^{-7}$  to  $10^{-6} \text{ m}$  in thickness on their surface. The layer is composed of densely packed individual crystallites  $10^{-7}$  to  $10^{-6} \text{ m}$  in size, with nanocrystallites  $10^{-9}$  to  $10^{-7} \text{ nm}$  in size forming on their surface under certain conditions. The crystallites on the surface of strontium titanate are pyramidal in shape and have a certain orientation of their crystallographic planes [31]. Plasma exposure leads to surface amorphisation of sapphire and garnet samples, with a degree of order in the surface distribution of the crystallites. Such results were obtained for both nominally undoped samples and samples doped with iron-group and lanthanoid ions. At the same time, the geometry, shape and degree of order of the crystallites clearly depend on their stoichiometry and impurity composition. Plasma exposure shifts the TiK $_{\alpha 1}$  line of strontium titanate to higher energies, which is due to the formation of additional  $Ti^{3+}$  ions on the sample surface (Fig. 10). It is reasonable to assume a  $Ti^{3+}$  concentration gradient along the nanocrystallites and the associated increase in conductivity at 'peaks'.

The mechanism behind the formation of arrays of pyramidal crystallites  $10^{-10}$  to  $10^{-8} \text{ m}$  in size, including ordered arrays, on the surface of oxide single crystals is not yet fully understood. This effect can easily be accounted for by surface layer sputtering in a plasma pulse field and crystallisation in an external magnetic field. The surface layer on ruby and garnet was amorphous and that on strontium titanate was polycrystalline, with well-defined orientation of the nanocrystallite surfaces. One obvious cause of the difference in surface structure between sapphire (garnet) and strontium titanate is the considerable difference in electrical conductivity, which also requires further investigation.

The present spectroscopic data lead us to conclude that sapphire, garnet, yttrium orthoaluminate and strontium titanate crystals doped with Ti, V and Cr have similar absorption spectra. The spectra contain only impurity bands of various strengths, redshifted because of the increased lattice parameter.

The study of the spectroscopic properties of strontium titanate, both perfect and nonstoichiometric, and theoretical calculations of the energy of electronic transitions of  $Me^{n+}$  ions on tetrahedral and octahedral lattice sites allow one to identify colour centres and optical absorption (luminescence) bands.

## 6. Conclusions

The main results of this study are as follows:

Plasma exposure of the surface of sapphire, garnet and strontium titanate single crystals leads to the formation of one-, two- or multilevel quasi-ordered structures. SEM and AFM images demonstrate that, after such exposure, the samples have a complex surface topography. The surface of strontium titanate single crystals has zones of quasi-ordered structures of pyramidal crystallites  $10^{-9}$  to  $10^{-7} \text{ m}$  in size. The number density of individual crystallites reaches  $10^{20} \text{ m}^{-2}$ . Plasma exposure of sapphire and garnet samples results in the formation of an amorphous surface layer with a crystallite size from  $10^{-9}$  to  $10^{-6} \text{ m}$  and a number density lower by several orders of magnitude ( $10^{10}$  to  $10^{18} \text{ m}^{-2}$ ).

After plasma exposure to various energy densities, the surface of a number of doped strontium titanate crystals had areas of two-level quasi-ordered structures  $10^{-7}$  to  $10^{-5} \text{ m}$  in size, with arrays of densely packed crystallites  $10^{-10}$  to  $10^{-8} \text{ m}$  in size on their surface. Micro- and nanostructures form in a rather wide range of plasma energy densities.

The IA spectra of irradiated chromium-doped crystals contain bands at  $\lambda \approx 217$ ,  $270$ ,  $360$  and  $460 \text{ nm}$  (ruby);  $230$ ,  $260$ ,  $290$ ,  $480$ ,  $640$ ,  $964$  and  $1100 \text{ nm}$  (YAG:Cr);  $250$ ,  $300$ ,  $400$ ,  $520$ ,  $660$  and  $1050 \text{ nm}$  (GSGG and other mixed garnets); and  $295$ ,  $385$ ,  $425$  and  $500 \text{ nm}$  (YAlO $_3$ :Cr). The bands at  $217$ ,  $270$ ,  $360$  and  $460 \text{ nm}$  (ruby);  $230$ ,  $290$ ,  $480$  and  $520 \text{ nm}$  (YAG:Cr); and  $250$ ,  $300$ ,  $400$  and  $520 \text{ nm}$  (mixed garnets) are due to transitions in  $Cr^{4+}:[O^{2-}]_6$  octahedral clusters. The bands at  $640$ ,  $964$  and  $1100 \text{ nm}$  (YAG:Cr) and  $504$ ,  $660$  and  $1050 \text{ nm}$  (mixed garnets) arise from transitions in tetragonal clusters.

A similar situation occurs in the case of vanadium-doped garnet crystals. Their IA spectrum has peaks at  $\lambda = 438$ ,  $590$ ,  $830$ ,  $1150$  and  $1300 \text{ nm}$ , due to transitions in  $V^{4+}:[O^{2-}]_6$  octahedral clusters ( $\lambda = 438$  and  $590 \text{ nm}$ ) and tetrahedral clusters ( $\lambda = 830$ ,  $1150$  and  $1300 \text{ nm}$ ).

The absorptions at  $\lambda = 430, 520$  and  $650$  nm in strontium titanate samples are due to  $\text{Ti}^{3+}$  electronic transitions. The 430-nm absorption band corresponds to  $4s \rightarrow 3d$  transitions, accompanied by luminescence at  $\lambda = 450$  nm. The  $3d \leftrightarrow 3d$  transitions of  $\text{Ti}^{3+}$  ions on lattice sites are responsible for the absorption at  $\lambda \simeq 520$  nm and luminescence at  $\lambda \simeq 650$  nm. The absorption band centred at  $\lambda = 650$  nm and luminescence around 700 nm are due to transitions in  $\text{Ti}^{3+}:\text{[O}^{2-}]_k$  clusters with  $k = 3$  and 4. Radiative colour centres are unstable under normal conditions because of the high permittivity of perfect crystals and considerable electrical conductivity of nonstoichiometric materials. At the same time, the IA spectra of a number of samples are fully consistent with transitions of  $\text{Ti}^{3+}:\text{[O}^{2-}]_k$ .

The present results lead us to conclude that the electronic structure and spectroscopic properties of oxide laser crystals can be controlled both during growth and by subsequent thermal annealing or exposure to ionising radiation or plasma.

**Acknowledgements.** I am grateful to A.V. Sandulenko (St. Petersburg) for his effective assistance with this study; to my colleagues at the Faculty of Physics of the University of Belgrade (Serbia), especially to J. Dojilovic and I. Dojcinovich; to E. Hieckmann from the Technische Universität Dresden (Germany) for her assistance with characterisation of the samples; and to I.E. Garkusha and the personnel of the Institute of Plasma Physics, Kharkiv Institute of Physics and Technology National Scientific Centre, National Academy of Sciences of Ukraine, for their assistance with the irradiations on a plasma compressor.

## References

- Kaminskii A.A. *Laser Crystals* (New York: Springer, 1981; Moscow: Nauka, 1975).
- Smolenskii G.A., Bokov V.A., Isupov V.A., et al. *Segnetoelektriki i antisegetoelektriki* (Ferroelectrics and Antiferroelectrics) (Leningrad: Nauka, 1985).
- Sviridov D.T., Sviridova R.K., Smirnov Yu.F. *Opticheskie spektry ionov perekhodnykh metallov v kristallakh* (Optical Spectra of Transition Metal Ions in Crystals) (Moscow: Nauka, 1976).
- Kulagin N.A., Sviridov D.T. *Vvedenie v fiziku aktivirovannykh kristallov* (Introduction to the Physics of Doped Crystals) (Kharkov: Vysshaya Shkola, 1990).
- Physics of Laser Crystals*. J.-C. Krupa, N.A. Kulagin (Eds.) (Bruxelles: Kluwer Acad. Publ., 2003).
- Kulagin N.A., Sviridov D.T. *Metody rascheta elektronnykh struktur svobodnykh i primesnykh ionov* (Electronic Structure Calculations for Free and Impurity Ions) (Moscow: Nauka, 1986).
- Men' A.N., Vorob'ev Yu.P., Shuvanov G.I. *Fiziko-khimicheskie svoystva nestekhiometricheskikh oksidov* (Physicochemical Properties of Nonstoichiometric Oxides) (Leningrad: Nauka, 1973).
- Krutova L.I., Kulagin N.A., Sandulenko V.A., Sandulenko A.V. *Fiz. Tverd. Tela*, **31** (1), 170 (1989).
- Kulagin N.A. *Opt. Spektrosk.*, **101** (2), 436 (2006).
- Lemanov V.V., Smirnova E.P., Syrnikov P.P., Tarakanov E.A. *Phys. Rev. B*, **545** (2), 151 (1996).
- Lemanov V.V. *Fiz. Tverd. Tela*, **39** (3), 1645 (1997).
- Lemanov V.V., Sotnikov A.V., Smirnova E.P., Weihnacht M., Haessler W. *Fiz. Tverd. Tela*, **441** (4), 1091 (1999).
- Bogatko V.V., Muromtsev V.I., Litvinov L.A., Venevtsev Yu.N. *Izv. Akad. Nauk SSSR, Ser. Neorg. Mater.*, **17** (10), 2229 (1981).
- Belyaev L.N. (Ed.) *Rubin i sapfir* (Ruby and Sapphire) (Moscow: Nauka, 1974).
- Dojilovic J., Kulagin N.A. *Fiz. Tverd. Tela*, **38** (7), 2012 (1996).
- Kulagin N.A., Dojilovic J. *Phys. B*, **269** (10), 1645 (1999).
- Mikhailov M.P., Kuleshov N.V., Zhavoronkov N.I., Prokoshin P.V., Yumashev K.V., Sandulenko V.A. *J. Opt. Mater.*, **2** (1), 267 (1993).
- Il'ichev N.N., Kir'yanov A.V., Pashinin P.P., Sandulenko V.A., Sandulenko A.V., Shpuga S.M., *Kvantovaya Elektron.*, **22** (12), 1192 (1995) [*Quantum Electron.*, **25** (2), 1154 (1995)].
- Malyarevich A.M., Denisov I.A., Yumashev K.V., Mikhailov V.P., Conroy R.S., Sinclair B.D. *Appl. Phys. B*, **67** (3), 555 (1998).
- Karlov N.V., Manenkov A.A. *Kvantovye usiliteli* (Quantum Amplifiers) (Moscow: Nauka, 1966).
- Kulagin N.A. *Mater. Sci. Forum*, **494** (1), 55 (2005).
- Kulagin N., Dojilovic J., Popovic D. *Cryogenics*, **41** (10), 745 (2001).
- Little F.W. *J. Appl. Phys.*, **35** (7), 2212 (1964).
- Fischer M., Lahmar A., Maglione M., et al. *Phys. Rev. B*, **49** (2), 451 (1994).
- Kulagin N.A. *Fiz. Tverd. Tela*, **25** (7), 392 (1983).
- Fischer M., Bonello B., Itie J., et al., *Phys. Rev. B*, **43** (12), 8494 (1990).
- Kulagin N.A., Ovechkin A.E. *Zh. Prikl. Spektrosk.*, **39** (3), 488 (1983).
- Kulagin N.A., Sviridov D.J. *J. Phys. (London)*, **C17**, 4539 (1984).
- Kulagin N.A., Litvinov L.A., Rokhmanova V.O. *Zh. Prikl. Spektrosk.*, **46** (5), 969 (1987).
- Kulagin N.A., Ozerov M.F. *Fiz. Tverd. Tela*, **35** (11), 2472 (1993).
- Kulagin N.A., Levin A.A., Langer E., Meyer D.C., Dojcinovich I., Puric J. *Kristallografiya*, **53** (6), 1061 (2008).
- Kulagin N.A., Hieckmann E., Dojilovic J. *Fiz. Tverd. Tela*, **52** (12), 2583 (2010).
- Kulagin N.A. *J. Lumin.*, **131** (1), 526 (2011).
- Kulagin N.A., Litvinov L.A. *Cryst. Res. Technol.*, **20** (6), 1667 (1985).
- Kulagin N.A., Dojilovic J., Popovic D., Spasovic S. *Kristallografiya*, **49** (6), 534 (2004).
- Kuraica M.M., Astashinski V.M., Dojcinovich I.P., Puric J., in *Physics of Laser Crystals* (Bruxelles: Kluwer Acad. Publ., 2003) p. 245.
- Puric J., Kuraica M.M., Astashinski V.M., Dojcinovich I.P. *Vacuum*, **73** (1), 261 (2004).
- Tereshin V.I., Garkusha I.E., Bandura A.N., Byrka O.V., Chebotaev V.V., Makhaj V.A., Solyakov D.G., Wuertz H. *J. Nucl. Mater.*, **313-316** (3), 685 (2003).
- Barinskii L.B., Nefedov V.I. *Rentgeno-spektral'noe opredelenie zaryada atomov i molekul* (Determination of the Charges on Atoms and Molecules by X-Ray Spectroscopy) (Moscow: Nauka, 1966).
- Bartram R.H., Swenberg C.F., Fournier J.T. *Phys. Rev.*, **139** (2), 941 (1965).
- Stoneham A. *Theory of Defects in Solid State* (London: McGraw-Hill, 1968).
- Kulagin N.A., Sandulenko V.A. *Fiz. Tverd. Tela*, **31** (1), 243 (1989).
- Sandulenko A.V., Kulagin N.A. *Opt. Spektrosk.*, **126** (3), 285 (2009).
- Kulagin N.A., Hieckmann E. *Opt. Spektrosk.*, **49** (1), 234 (2012).
- Kulagin N.A. *Fiz. Tverd. Tela*, **25** (11), 3392 (1983).
- Kulagin N.A., Sandulenko V.A., Korostel' L.A. *Abstr. VIII Int. Meeting Ferroelectricity* (Maryland, 1993) p. 428.
- Kulagin N.A., Korostel' L.A., Sandulenko V.A., Konstantinova A.F. *Izv. Akad. Nauk, Ser. Fiz.*, **58** (1), 21 (1994).
- Kulagin N.A., Troyan-Golovyan G.N. *Opt. Spektrosk.*, **74** (1), 14 (1993).
- Konstantinova A.F., Korostel' L.A., Kulagin N.A. *Kristallografiya*, **40** (8), 885 (1995).

50. Konstantinova A.F., Korostel' L.A., Sul'yanov S.N. *Kristallografiya*, **43** (5), 903 (1998).
51. Doichinovic I., Dojcilovic J., Popovic D., Puric J., Kulagin N.A. *Proc. Fall MRS 2006* (Boston, 2007) p.1278.
52. Kulagin N.A., Dojcilovic J., Hieckmann E. *Mater. Sci. Applic.*, **2** (8), 971 (2011).
53. Sumbaev O.I. *Usp. Fiz. Nauk*, **124** (2), 281 (1978).
54. Vo Chiong Ki, Zaitseva Yu.V., Kulagin N.A., Podus L.P. *Fiz. Tverd. Tela*, **26** (12), 3521 (1984).
55. Kulagin N.A. *J. Solid State Chem.*, **78** (2), 555 (2005).
56. Hartree D. *Atomic Structure Calculations* (London: J. Wiley, 1957).
57. Kulagin N.A. *Fiz. Tverd. Tela*, **44** (6), 1421 (2002).
58. Kulagin N.A. *Physica B*, **222** (1), 173 (1996).
59. Nikitin A.A., Rudzikas Z.B. *Osnovy teorii spektrov atomov i ionov* (Introduction to the Theory of Spectra of Atoms and Ions) (Moscow: Nauka, 1973).
60. Kulagin N.A. *J. Phys. B*, **16** (10), 1695 (1983).
61. Kulagin N.A. *J. Phys. B*, **28** (3), 373 (1995).